Interaction Notes

Note 485

25 October 1991

ON THE INTERACTION OF ELECTROMAGNETIC FIELDS WITH WIRE CAGE STRUCTURES

M. Nyffeler, B. Braendli, B. Reusser, and E. Doerr
NC Laboratory, Spiez, Switzerland

and

D.V. Giri and E.R. Tomer
Pro- Tech, 3708 Mt. Diablo Boulevard, Suite 215, Lafayette, CA 94549-3610

Abstract

In this paper we address the problem of the interaction of electromagnetic fields with wire cage structures. The two canonical shapes considered are cubes and cylinders. The motivation for this work comes from a need to investigate electromagnetic field coupling (transient or broadband CW) to communication facilities or buildings with metallic rebar elements in the perimeter walls. Coupling calculations are performed by using NEC-2 computer codes, and the experiments were performed at the Swiss MEMPS facility. MEMPS is a hybrid type of NEMP simulator consisting of an impedence loaded elliptical structure with either a transient or broadband CW excitation. Both types of excitations have been used in experimentally studying the coupling characteristics. In the case of cylindrical wire cage structures, both polarizations i..e., incident electric field and incident magnetic field parallel to the cylinder axis, have been investigated. Good agreement is seen between the computed and measured results.

Preface

The authors are thankful to Defense Technology and Procurement Agency (DTPA), Federal Government of Switzerland for making available the NEMP simulator facilities at NC Laboratory, Spiez, where the broadband CW and transient experiments were performed. We are also grateful to Dr.M.Keller of NC Laboratory for his encouragement and support. Thanks are also due to Dr.Fred Tesche for valuable discussions relating to data processing.

Contents

1. Introduction

There appears to be a continued interest in the interaction of nuclear electromagnetic (NEMP) [1,2] fields with buildings and facilities that contain electronic systems when such buildings have metallic rebar elements in the perimeter walls. The actual coupling characteristics for any given building depend on the illuminating fields, the size and shape of the building, the rebar parameters etc. However, in order to gain an understanding of the interaction and coupling mechanisms, it is useful to study certain canonical wire cage structures. A second objective of studying interaction with canonical objects is to experimentally validate the selected computational model. Once thus validated, the computational model can be applied with increased confidence to actual buildings. The illuminating fields used in our computational models are that of a plane electromagnetic wave with a prescribed angle of incidence and polarization. The illuminating fields in our experimental studies are the simulated fields in a hybrid type of an NEMP simulator i.e., the Swiss MEMPS. MEMPS is basically an impedance loaded elliptical structure that can be energized either by a transient pulse generator or a suitable CW source. Both of these source types have been used in our experimental studies.

Researchers in the past have considered electromagnetic scattering by single wire meshes [3,4,5] and two perpendicular wire meshes [6], both in freespace and also over conducting half space. Shielding properties of certain types of buildings, e.g., residences with woodframes, concrete blocks with steel frames, multistory office buildings with steel frames etc., have been reported [7]. Numerical computations of electromagnetic pulse penetration into reinforced-concrete buildings, have also been reported [8]. The building is modelled by parallel wires , and time domain electric field integral equations are solved via the method of moments. Methods of enhancing the shielding effectiveness provided by a reinforced concrete facility have also been suggested [9]. These papers [3 to 9] attest to the fact that the problem of extraneous electromagnetic interference e.g., lightning, NEMP, radio / radar / EW transmitters etc., is growing. Correspondingly, the need for well shielded facilities that are also cost effective has increased. The objective of the present paper has been two fold. One needs to select a computational model that provides reasonably accurate results, and then validate such a model by carefully designed experiments. These are the distinguishing features of the present work. Two canonical shapes i.e.,cubes and cylinders have been chosen for both computational and experimental investigations. The sizes and shapes of the test objects, the illuminating fields in theory and in practice, the results of the computational model, and the experiment and their comparisons are all described in the following sections.

2. Canonical Wire Cage Structures

The selected canonical shapes for our investigations are cubes and cylinders. The cube is 2m on a side while two sizes are considered for the cylinder. These are: (a) 2m in length and 2m in diameter, and (b) 4m in length and 2m in diameter. Both of these cylinders have end caps . The 2m cube with 5 segments to a side is shown in figure 1, whereas the canonical segmented cylinder is shown in figure 2. In general a CUBE-N has N segments to a side, and it can be shown that a CUBE-N has (12 NxN) segments in total. Consequently, CUBE-5 has exactly 300 segments. The segment length in our experimental CUBE-4 was 0.5m. In both cases a rectangular coordinate system with its origin at the center of the test object (cube or cylinder) is defined, in such a way that none of the three axes intersect the wire segments. This featute helps in avoiding field computation on a wire segment. It is noted that the design of the end caps, in the case of the two cylinders is also such that the cylinder axis coincides with a coordinate axis and does not intersect any wire segment

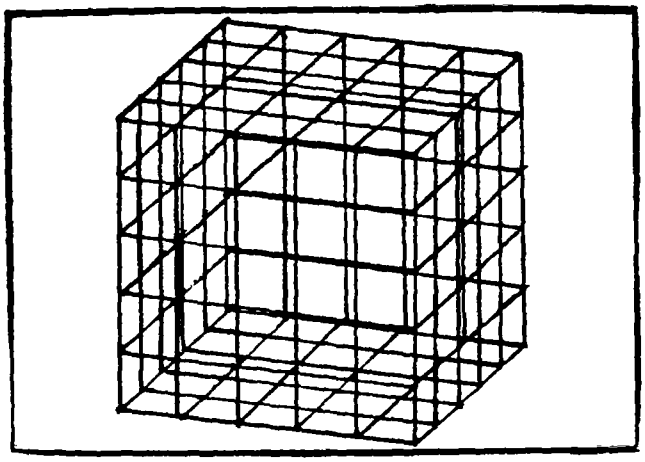

Figure 1. Illustration of a CUBE-5, which is 2m long on all sides with 5 segments (0.5m long) per side

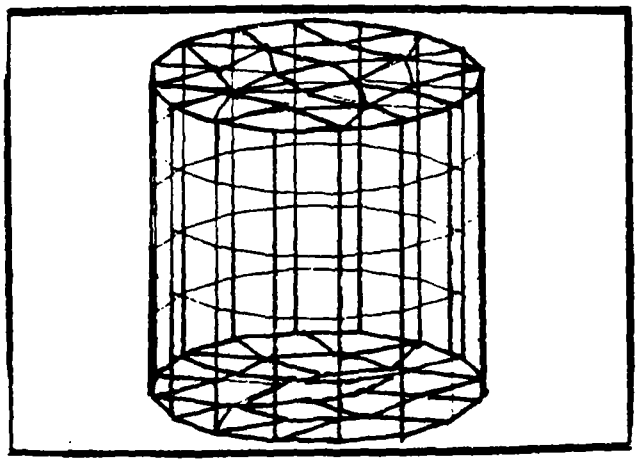

Figure 2. Illustration of a cylinder which is 2m long and 2m in diameter (The end caps and the segmentation along the axial direction is such that segment lengths vary in the rang e of 0.35000m to 0.50168m)

of the end cap. There is no loss of generality in these choices. Only the 2m long cylinder is shown in figure 2, and it has a total of 272 segments. The 4m long cylinder is simply made of two such cylinders with identical end caps .While the cube is a symmetric structure thus requiring only one incident polarization, the cylinder has been analyzed in theory and experiment with two possible incident polarizations. These are incident electric and magnetic field parallel to the cylinder axis respectively. The coordinate system and the various incident polarizations are illustrated in figure 3. In the context of the cube, the incident magnetic field is in the +x direction, the incident electric field is in the -z direction and the direction of incident wave propagation is along the -y axis as illustrated in figure 3a. Figure 3b and 3c respectively illustrate plane wave incidence on the cylinder with the incident electric and magnetic fields parallel to the cylinder axis.

It is also noted that the individual wire segments are metallic strips, galvanized steel in the case of the cube, and cast iron in the case of the cylinders. In the computational models, equivalent radii are used in approximating the segments by round conductors. The end caps are located on the cylinders at z = +1m and -1m for the 2m cylinder and, at z = +2m and -2m for the 4m long cylinder. The wire segments in the end caps are triangulated. One quarter of the end cap is shown in figure 4 and each cap is seen to consist of 36 triangles plus 1 square at the center. The final cylinder geometry is rotated by 11.25 degrees, so that none of the observation points lie on a wire segment. This completes a brief description of the wire cage structures that have been studied here.

3. Incident Fields

In this section, we briefly describe the illuminating electromagnetic fields for the three cases illustrated in figure 3.

a) 2m Cube; CUBE-4; 4 segments per side; total of 192 wire segments

$$\vec{E}_{inc} = -\vec{1}_z E_o e^{jky} \; ; \; \vec{H}_{inc} = \vec{1}_x H_o e^{jky}$$
$$\text{where } E_o = 1 \text{ V/m, and } H_o = E_o / Z_o = 2.653 \text{ mA/m} \qquad (1)$$

The above listed illumination is used in the frequency domain computations performed with NEC-2 , described in the following section. In the CW experiments, the incident field is effectively of constant magnitude when we reference the interior fields to the incident field. In the experimental case of pulsed excitations, the incident electric and magnetic field waveforms as a function of time, at the center of the test object are measured, before positioning the test objects. The MEMPS pulser is operated at 1.4 MV level, resulting in a peak electric field amplitude of about 40 kV/m at the center of the test objects. The actual experimental configurations are described in a later section.

b) 2m long, 2m diameter cylinder; total of 272 segments

$$\vec{E}_{inc} = -\vec{1}_z E_o e^{jky} \; ; \quad \vec{H}_{inc} = \vec{1}_x H_o e^{jky} \quad \text{(E - parallel)}$$
$$\vec{H}_{inc} = -\vec{1}_z H_o e^{jky} \; ; \quad \vec{E}_{inc} = -\vec{1}_x E_o e^{jky} \quad \text{(H - parallel)}$$
$$H_o = (E_o / Z_o) \text{ A/m with } E_o = 1 \text{ V/m} \qquad (2)$$

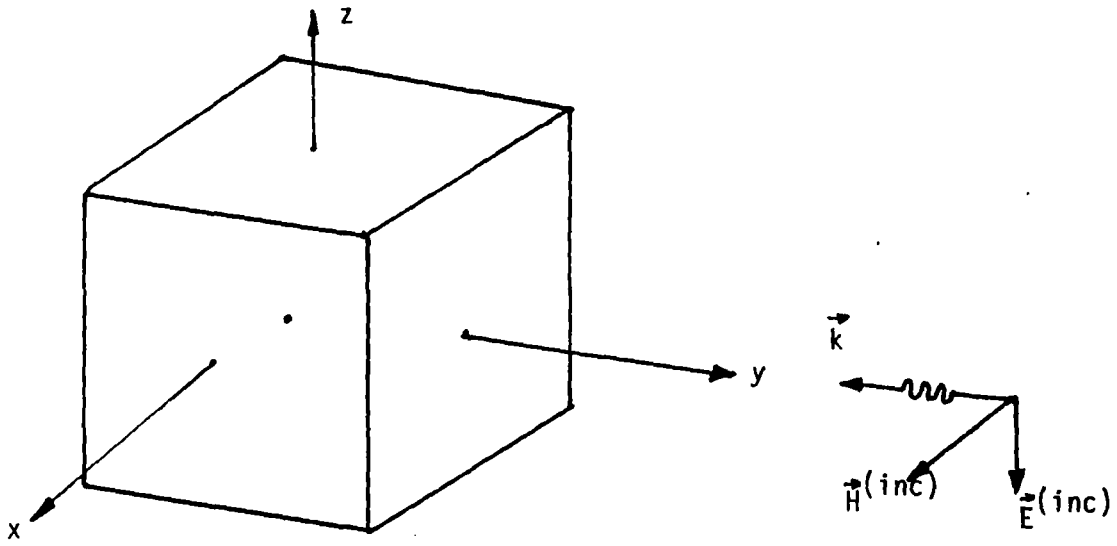

a) wave incidence on a segmented cube

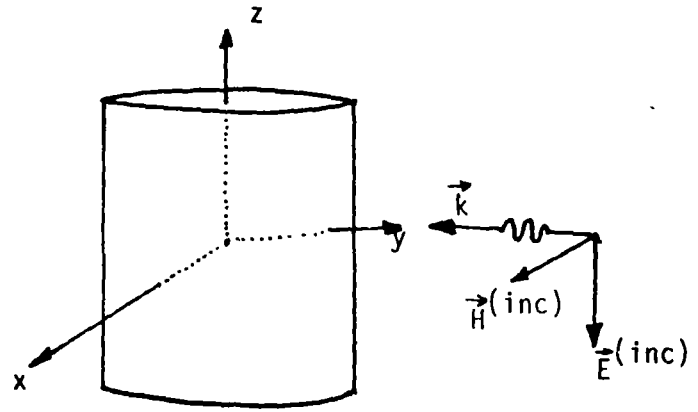

b) wave incidence on a segmented cylinder (E-parallel)

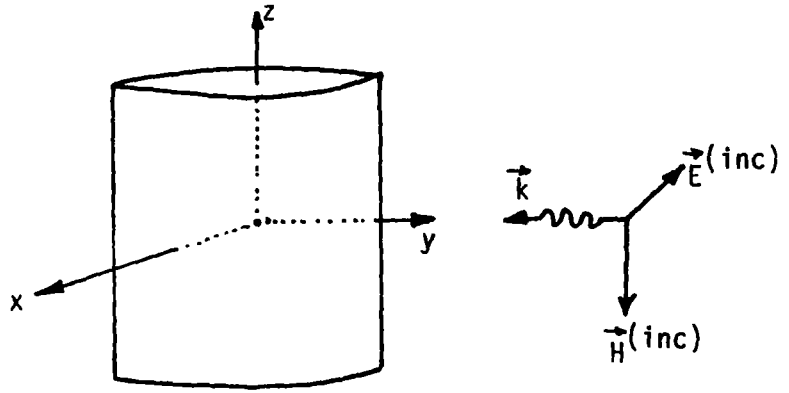

c) wave incidence on a segmented cylinder (H-parallel)

Figure 3. The rectangular coordinate system and various incident wave polarizations

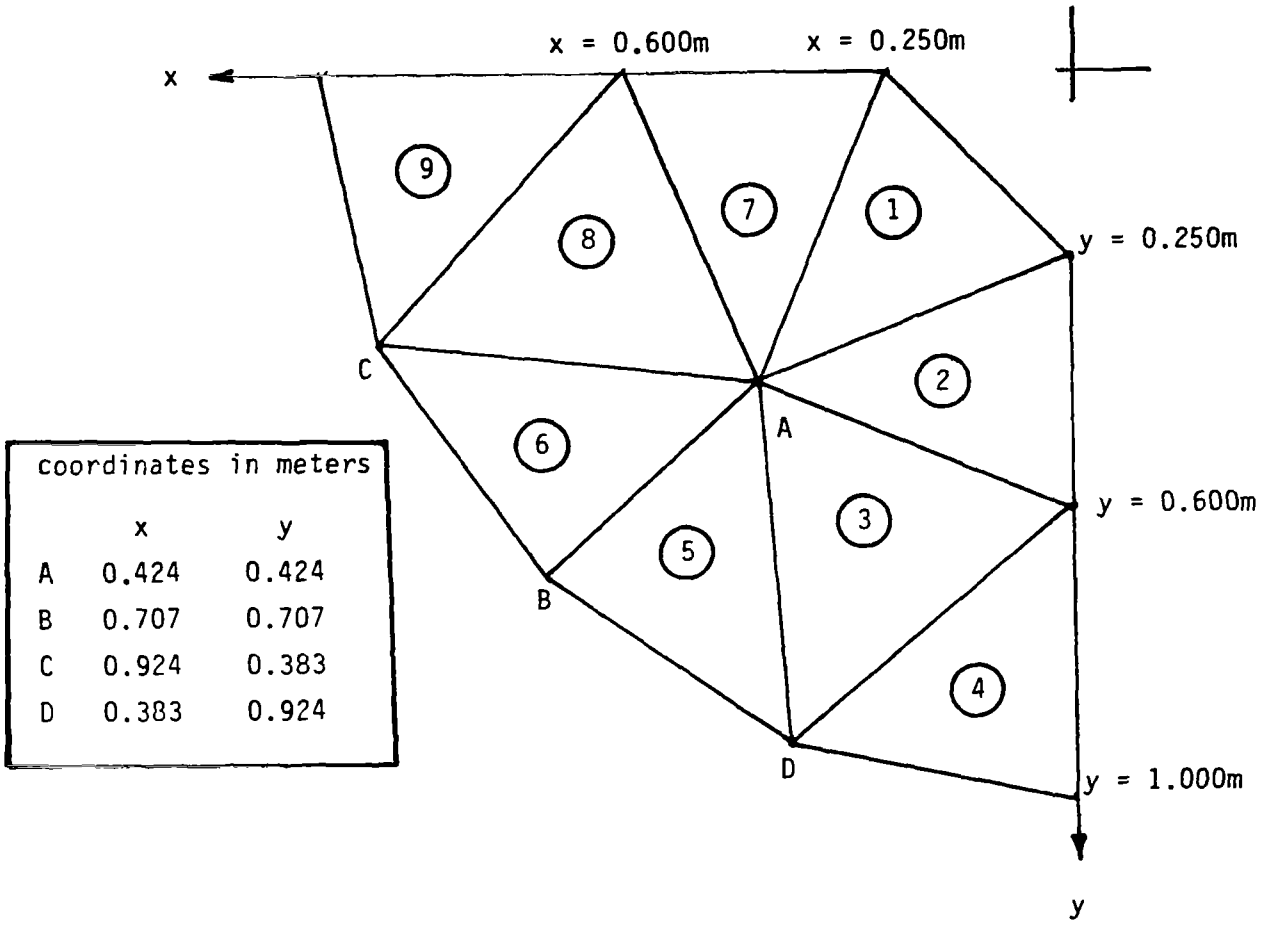

coordinates in meters		
	x	y
A	0.424	0.424
B	0.707	0.707
C	0.924	0.383
D	0.383	0.924

Figure 4. Diagram of one quarter of the cylinder end cap triangulation

c) 4m long, 2m diameter cylinder; total of 432 segments

same incident field as in case (b) above for the two polarizations of E-parallel and H-parallel to the cylinder axis (i.e., + z coordinate axis).

4. Computational Model

The fields that penetrate the wire cage structures are computed in the frequency domain by using the NEC-2 computer codes [10,11,12] that are commercially available. The numerical electromagnetic code (NEC) is a frequency domain code applying the method of moments technique [13] to solve integral equations for wire and surface structures that represent antennas or scatterers. For the present application of computing the scattered fields inside the wire cage structures, NEC-2 initially solves for the current distributions on all of the wire segments . This is done by solving the electric field integral equation . Under the thin wire approximation, this integral equation is given by

$$\int_C I(\xi')\left[k^2 \vec{l}_\xi . \vec{l}_{\xi'} - \frac{\partial^2}{\partial\xi\partial\xi'}\right] g(\vec{r},\vec{r}')\,\partial\xi' = \left(\frac{-j4\pi k}{Z_o}\right) \vec{l}_\xi . \vec{E}_{inc}(\vec{r}) \qquad : \vec{r} \in C(\xi)$$

where

$g(\vec{r},\vec{r}') = \exp(-jk\,|\vec{r}-\vec{r}'|)\,/\,|\vec{r}-\vec{r}'|$

$k = \omega\sqrt{\mu_o\varepsilon_o}$; $Z_o = \sqrt{\mu_o/\varepsilon_o}$

$I \equiv$ induced current ; $\vec{E}_{inc} \equiv$ incident field

$\vec{l}_\xi$, $\vec{l}_{\xi'} \equiv$ unit vectors tangent to the wire at ξ and ξ'

$\vec{r}$, $\vec{r}' \equiv$ vectors to the points ξ and ξ' on the wire contour $\vec{C}$ (3)

The above integral equation is solved numerically in NEC-2 by a form of the method of moments. Wires are divided into short straight segments, and the test functions are chosen to be delta functions in the collocation method of solutions.The expansion functions for the current on the various wire segments are chosen such that the total current on the jth segment has the form [14],

$$I_j(\xi) = A_j + B_j \sin\{k(\xi-\xi_j)\} + C_j \cos\{k(\xi-\xi_j)\} \qquad |\xi-\xi_j| < \Delta_j/2 \tag{4}$$

where

$\xi_j \equiv$ value of ξ at the center of segment j

$\Delta_j \equiv$ length of segment j

The coefficients (A, B and C's) are so related that the current distributions on various segments satisfy certain physical conditions on the current and charge at segment ends. These conditions together with the method of moments equations are adequate to evaluate all the individual wire segment currents (j = 1 to N, where N is the total number of segments) in the form of (4). Once the segment current distributions are evaluated, the electromagnetic fields are then determined by an

integration of these currents with appropriate Green's functions.

NEC-2 has been run for the two cylinders and the cube, under the thin wire approximations. These are: 1) transverse currents are negligible compared to axial currents, 2) azimuthal variation of the axial currents is negligible, 3) the current is representable by a filament on the axis, and 4) the boundary condition on the electric field need be enforced in the axial direction only. These conditions along with the postulated three term form of the segment current lead to a minimum and maximum segment length in terms of wavelengths.

The modeling guidelines laid down in the NEC-2 User's guide are strictly adhered to. The cube has a uniform segmentation of 0.4 m, while the cylinder segmentation varies from 0.35000 m to 0.50168 m. These parameters easily permit a maximum excitation frequency of 64 MHz. At the lower end, there is also a limitation on the excitation frequency stemming from the degeneracy of the constant and the coefficient of the cosine term in the current distribution. We have experienced no difficulty in computing the penetrant electromagnetic fields at frequencies down to 10 kHz for the electric field and 100 kHz for the magnetic field.

Initially, the excitation frequency is stepped through in this band of (100kHz to 64 MHz) and all six components of the scattered electromagnetic field are computed using NEC-2, along the three axis. The observation locations on the three axes, extend beyond the 2m cube and the 2m cylinder, so that one could even observe the changing scattered or total field as we move from the interior to the exterior regions of the test object. For the three test objects, several excitation frequencies were considered, and the scattered fields computed. Representative sample calculations of a cylinder (2m long and 2m diameter) at two frequencies of 1MHz and 32 MHz are shown in figures 5,6 and 7. In all of these cases, the polarization of the incident field is such that the incident magnetic field is parallel to the cylinder axis. The scattered magnetic field, computed with NEC-2 along the three axes are shown plotted in figures 5, 6 and 7 at excitation frequencies of 1 and 32 MHz.

One can get the total field by simply adding the incident field vectorially to the scattered field, recalling that the incident electric field has a value of 1 V/m in the computations, while the incident magnetic field has an amplitude of 2.653 mA/m as indicated in (1). The shielding effectivenesses may then be computed using the following general formulae

$$\text{SE (electric)} \equiv \eta^{e}(x,y,z,f) = 20 \log_{10}\left|\frac{E_{tot}(x,y,z,f)}{E_{inc}(x,y,z,f)}\right|$$

$$\text{SE (magnetic)} \equiv \eta^{m}(x,y,z,f) = 20 \log_{10}\left|\frac{H_{tot}(x,y,z,f)}{H_{inc}(x,y,z,f)}\right|$$

where

$$E_{tot} = \text{principal component of } (E_{scat} + E_{inc})$$
$$H_{tot} = \text{principal component of } (H_{scat} + H_{inc}) \qquad (5)$$

It is noted that the principal component of the computed scattered electric or magnetic field is in the same direction as the incident electric or magnetic field. As an example, we may illustrate a shielding effectiveness calculation, using the results in figure 5b,

$$\eta^{m}(0,0,0,32\text{MHz}) = 20 \log_{10}\left|1 + \frac{H_z^{(scat)}}{H_z^{(inc)}}\right| = 20 \log_{10}\left|1 - Z_o H_z^{(scat)}\right|$$

$$\equiv 20 \log_{10}\left|1 - 376.98 \times 2.329 \times 10^{-3}\right| = -18.27 \text{ db} \qquad (6)$$

This completes a brief description of the calculational model and representative results.

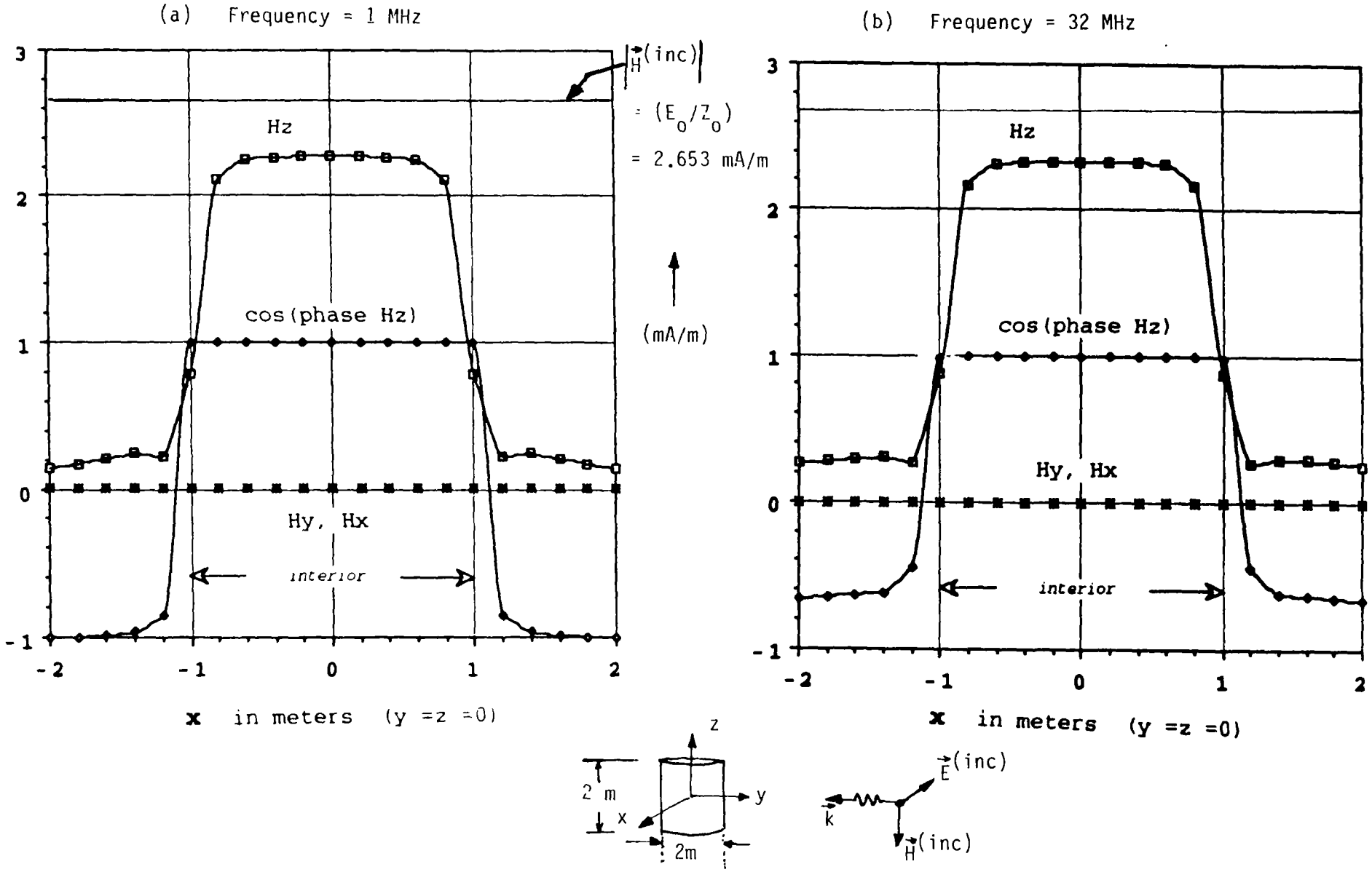

Figure 5. Computed scattered magnetic fields along the x axis for a segmented cylinder (2m long; 2m diameter; 272 segments) with the incident magnetic field parallel to -z axis

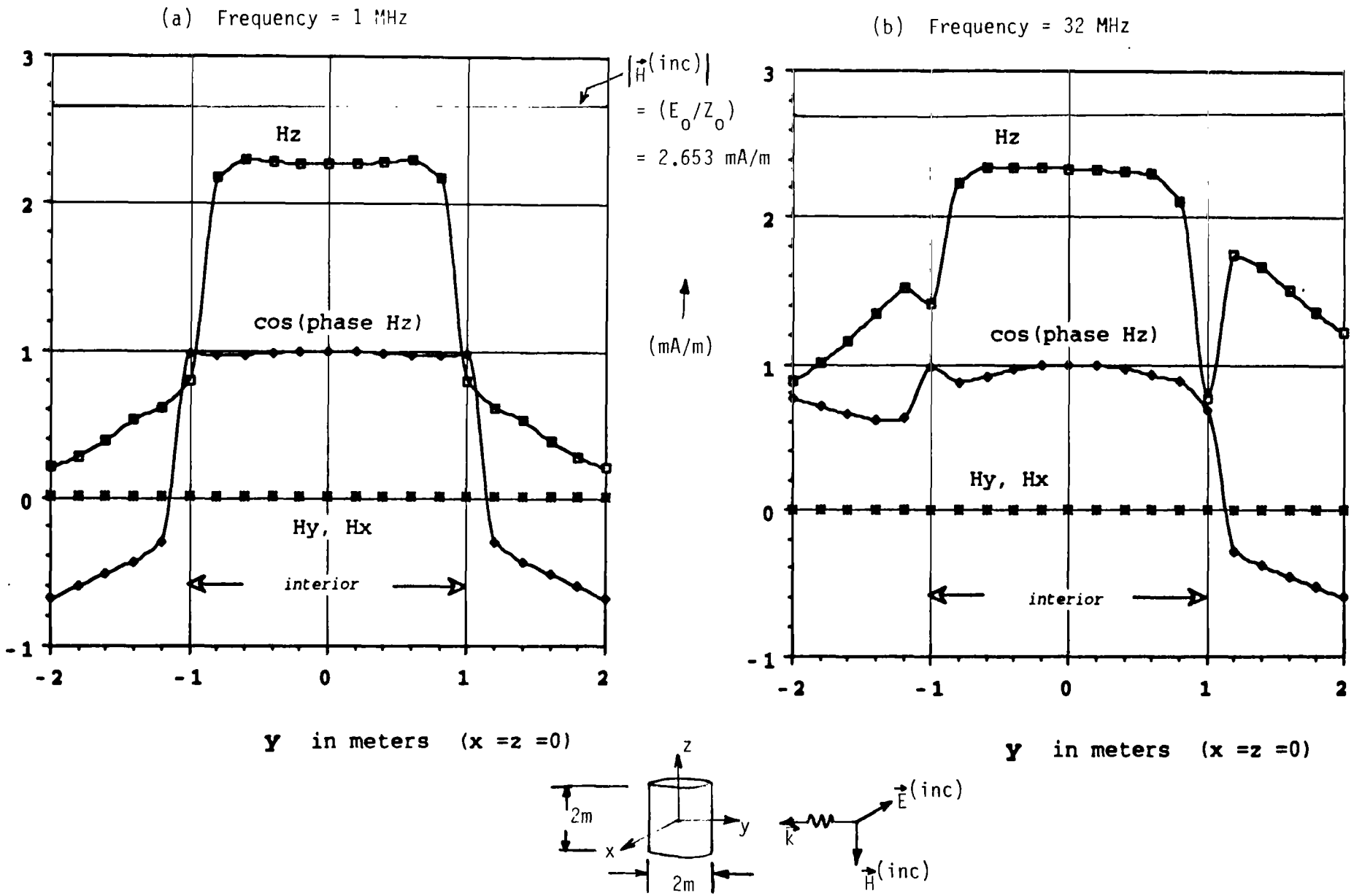

Figure 6. Computed scattered magnetic fields along the y axis for a segmented cylinder (2m long; 2m diameter; 272 segments) with incident magnetic field parallel to -z axis

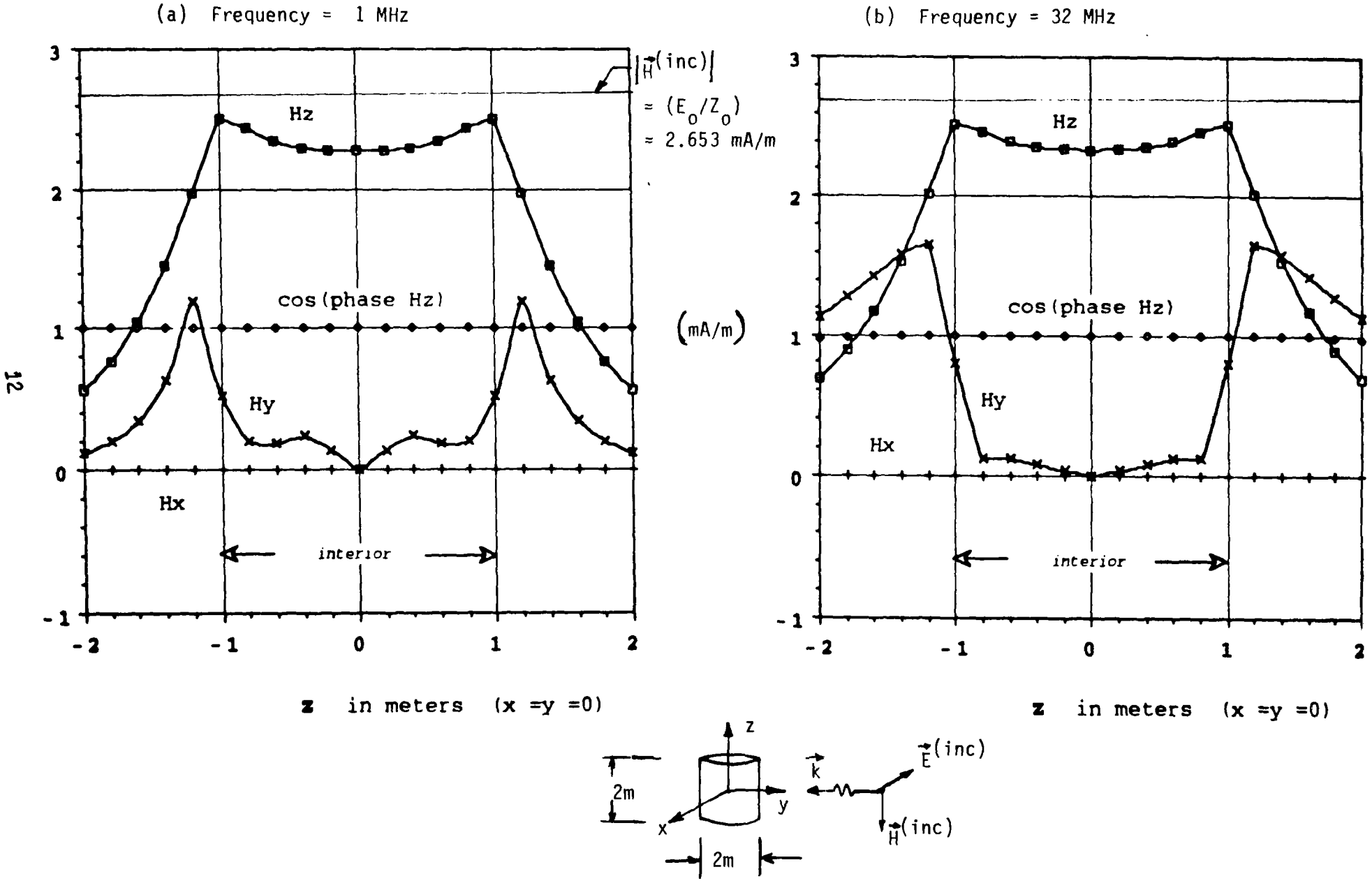

Figure 7. Computed scattered magnetic fields along the z axis for a segmented cylinder (2m long; 2m diameter; 272 segments) with incident magnetic field parallel to the -z ax

5. Experimental Studies

The experiments of electromagnetic wave coupling to wire cage structures have been performed in a hybrid type of NEMP simulator. This simulator is the Swiss MEMPS located at the NC Laboratory in Spiez, Switzerland. TheMEMPS [15, 16] is an example of an impedance loaded semi-elliptical wire structure above ground that has been routinely used in NEMP simulation. The major and minor axes of MEMPS are 60m and 40m respectively while the tubular wire cage that makes up the ellipse has an effective radius of 1.67m and the impedance loading is 1000 Ohms in the full ellipse. Both CW and transient pulser excitation are possible in MEMPS, and have been employed in our experiments. The test objects used in our experiments are shown in figure 8 and,as an example, the 4m long segmented cylinder is shown in figure 9 under the two different excitation configurations of the incident electric and magnetic fields parallel to the cylinder axis. The CW source seen in figure 9 is located at a height of 20 m above ground and the test objects are centered at a height of 8m above ground, so that the distance from the source to the test object is typically about 12m. Initially, the principal components of the incident electric and magnetic fields are measured at selected locations in the interior region of the test object with a CW source. A dielectric boom about 8m in height is used in measuring the incident fields. Then the test object is placed in the proper orientation and the measurements of the principal components of the total (scattered + incident) fields are made. The schematic diagram of the experimental setup is shown in figure 10 for the CW measurements. They are performed using a network analyzer with fiber optics for transmitting the measured data from the sensor location to the recording instrumentation. The broadband power amplifier and its primary power source (e.g., a diesel generator) are located in a shielded volume of the biconical surface, and it is turned on by a fiber optically transmitted signal sent by the operator in the shielded room, physically away from the facility.

The measurements were also repeated using a transient pulse generator that produced a double exponential pulse which is approximately represented by the following mathematical model

$$V_p(t) = V_o\,(e^{-\alpha t} - e^{-\beta t})\,u(t)$$

$$\text{with}\quad V_o = 1.4\ \text{MV}\ ;\ \alpha = 4\times10^6\ /\,\text{s}\ ;\ \beta = 480\times10^6\ /\,\text{s} \qquad (7)$$

The values of the rise and fall parameters in the above model are only indicative of the rise and fall times of the pulser output. A knowledge of the exact values of these parametrs is not critical, since the present interest is in the shielding effectiveness, which is basically the penetrant field for unit incident field. The measured time domain interior fields are Fourier transformed and then divided by the incident field spectrum, in computing the shielding effectiveness from the measured data. Shielding effectiveness derived from the measurements in CW and pulse modes are then compared with the calculated values from the previous section.

There were no serious problems experienced with the measurements in the CW mode, but in the pulse mode, one has to account for factors such as: a) shot to shot variations in the pulser, since the field measurements with and without the test object have to be necessarily made with separate pulser firings, b) inadequacy of late-time data leading to errors in the low frequencies, typically below 100 kHz, c) high frequency noise introduced by the fiber optic links, which may also vary from shot to shot. Corrections were made to the incident field to account for the shot to shot variations,by monitoring the incident field with a reference sensor. In the context of problem (b) above, it is noted that at late times, the incident field is falling exponentially, while the field inside the structure is still ringing down. Attempts to make corrections by adding exponential tails to the incident field at late times were made, but the results are not satisfactory below 100 kHz. This is a low frequency limitation in the pulse mode operation. In view of problem (c) above, the results of pulse mode operation are strictly valid from about 100 kHz to about 50 MHz.

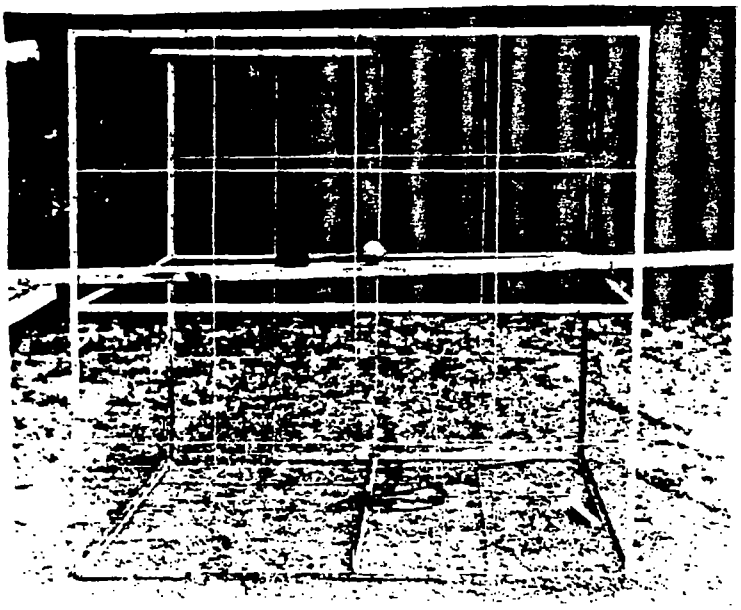

(a) 2m cube; 0.5m segmentation
192 segments

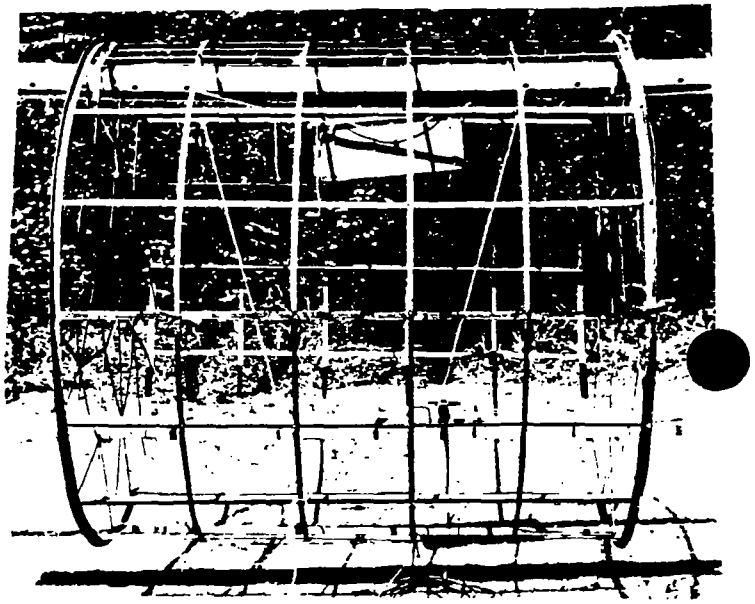

(b) segmented cylinder
2m long; 2m diameter
272 segments

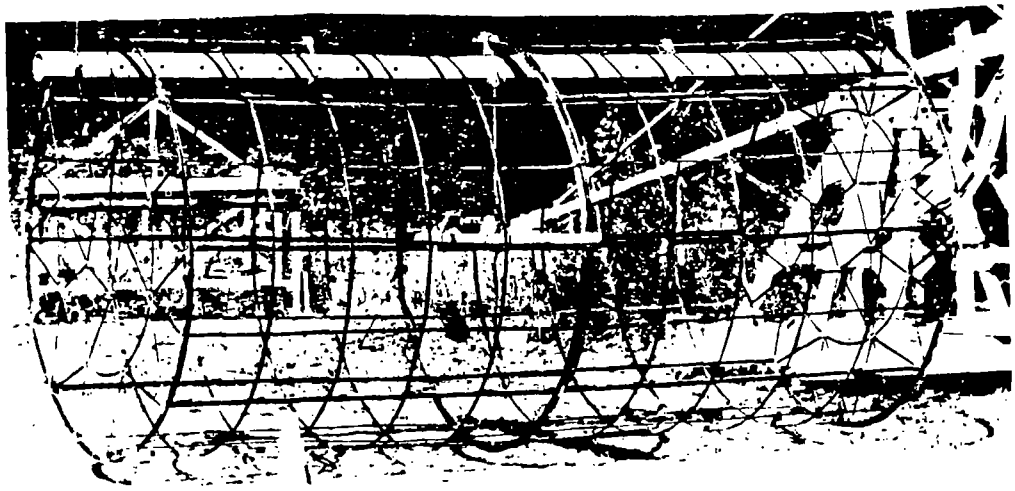

(c) segmented cylinder
4m long; 2m diameter
432 segments

Figure 8. Test objects

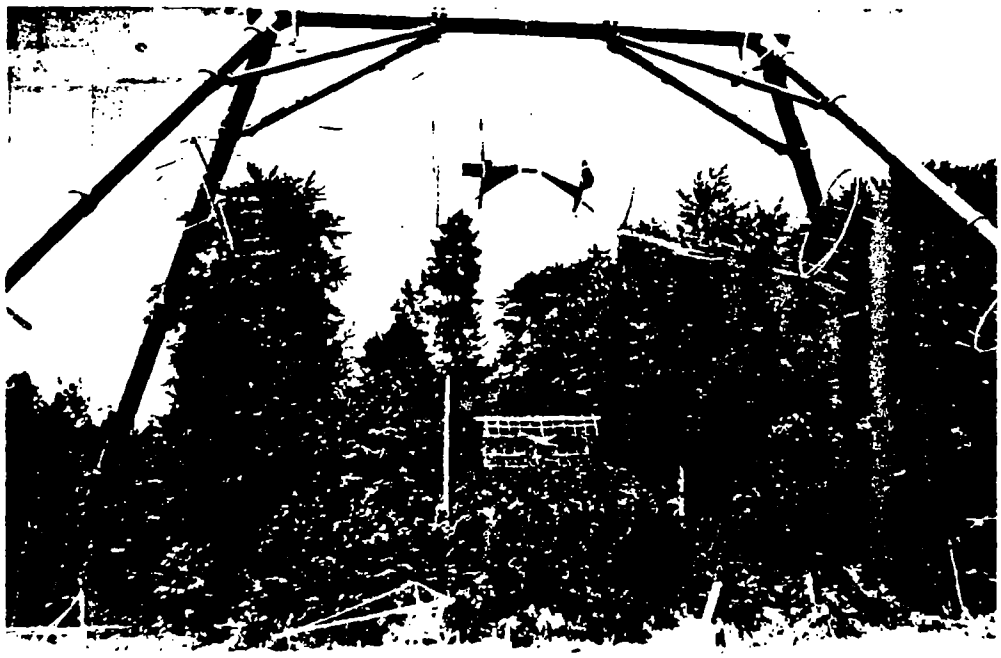

(a) CW excitation of the 4m cylinder with incident electric field parallel to the cylinder axis

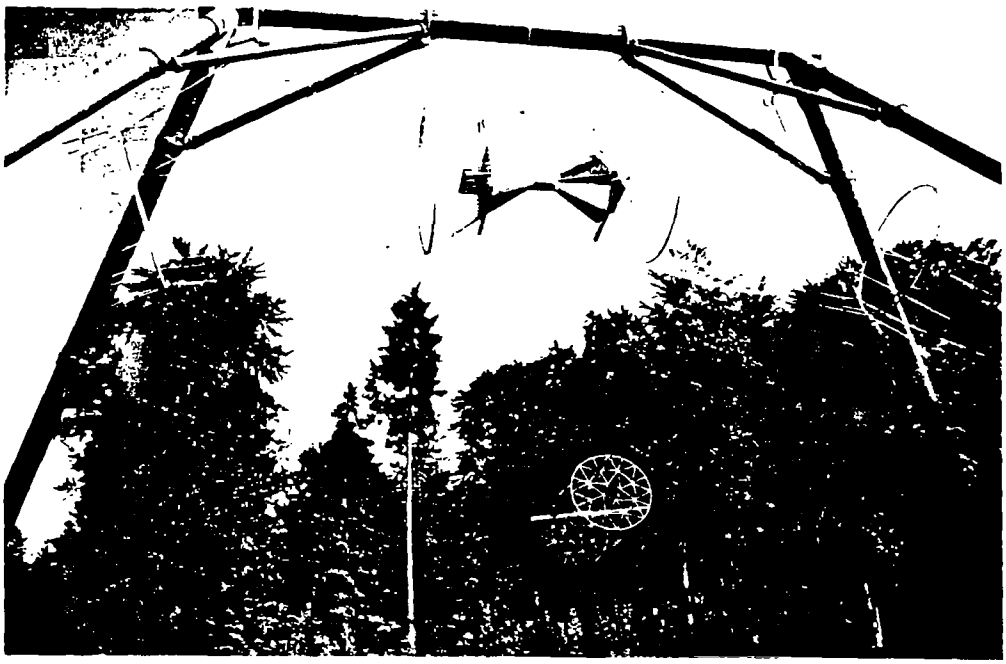

(b) CW excitation of the 4m cylinder with incident magnetic field parallel to the cylinder axis

Figure 9. Representative experimental configurations

CW-System MEMPS

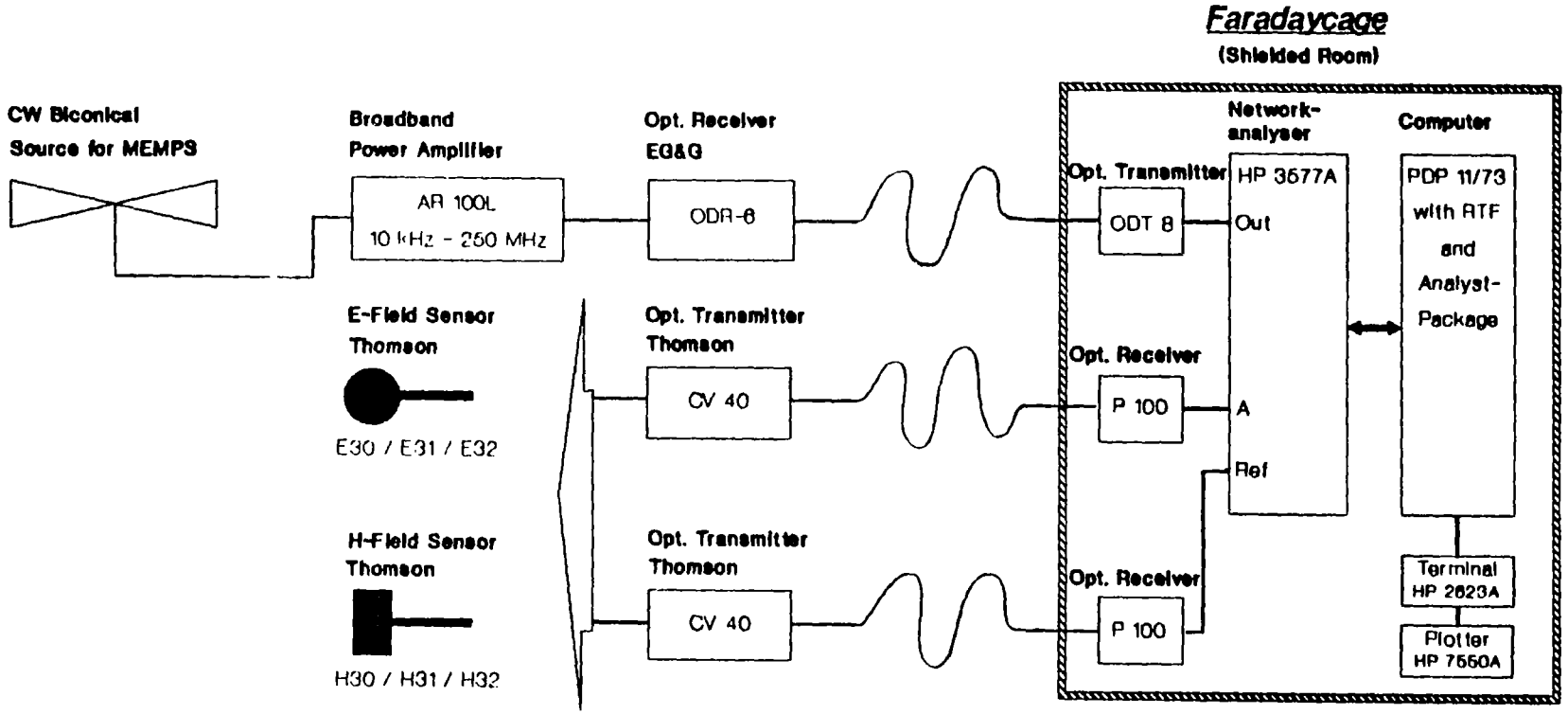

Figure 10. Experimental setup for the CW measurements of the incident/total electromagnetic fields

6. Comparison of Computed and Experimental Results

Using the computational model described earlier, we have evaluated the scattered and total fields (all six components), and the shielding effectivenesses for the following objects and incident polarizations:

1 to 6) CUBE - N with 12 N x N segments for N = 1 to 6
7,8) 2m long, 2m dia. cylinder ; 272 segments (0.4m long)E-parallel and H-parallel incidence

9,10) 4m long, 2m dia.cylinder; 432 segments(0.4m long) E-parallel and H-parallel incidence

It is noted that the experiments were performed for cases numbered 4 (i.e., CUBE-4), 7, 8, 9 and 10 above. Although the computations are made for various quantities such as all six components of the scattered fields, it has generally been found, both in the computation and experiment that the principal components of the electric and magnetic fields in the incident wave are also the dominant components of the scattered or the total fields in the interior volume of the structures. The incident wave is assumed to be an ideal plane wave in the calculations and was found to be nearly uniform at several measurement points in the volume occupied by the test objects. Furthermore, since we focus our attention on the shielding effectivenesses, which are basically field ratios, the non-planarity of the experimental incident wave is not critical .

In figure 11, the computed electric and magnetic shielding effectivenesses for six different cubes are plotted as a function of frequency . The frequency is varied from 10 kHz to an upper cut off frequency, that depends on the segment length, which is (2 m / N). The segment length for the six cubes ranges from 2m for CUBE-1 down to 33. 33 cm for CUBE-6. Since the segment length is required to be no larger than a tenth of the shortest wavelength, the upper cut off frequency is seen to range from 15 MHz for CUBE-1 to 90 MHz for CUBE-6. As may be expected, both the electric and magnetic shielding effectivenesses increase with N. It is also observed that at low frequencies the electric shielding effectiveness is relatively higher than its magnetic counterpart, as one may expect. We also experienced difficulties in computing low frequency magnetic fields using NEC-2. These problems were typically below 200 kHz. A general feature of these curves is that the shielding effectiveness is fairly constant at low frequencies and tends to have a relatively large notch in 20-40 MHz regime and then is an increasing function of frequency. This behavior is similar to EMP coupling through cable shields [17], where the dominant coupling mechanism at low frequencies is diffusion . The dominant coupling mechanism at high frequencies is aperture penetration and the crossover frequency in cable shield is typically around one MHz. Plots of the transfer impedance magnitude versus frequency that are presented in [17] show a behavior similar to the shielding effectivenesses computed or measured in the present work.

Next, we compare the calculated electric and magnetic shielding effectivenesses for the case of CUBE-4 (i.e., 2m cube with 50cm segmentation and a total of 192 segments) with the results from CW and pulse excitations in figure 12. Figure 12a, shows the electric shielding effectiveness while figure 12b shows the magnetic. As may be expected, relatively speaking, low frequency magnetic fields penetrate the structure easier than the electric fields. Notches in electric and magnetic shielding effectivenesses may be found at different interior locations and at different frequencies of excitation. The computations are carried up to a maximum frequency of about 60 MHz where the segment length of 0.5 m becomes a tenth of a wavelength.

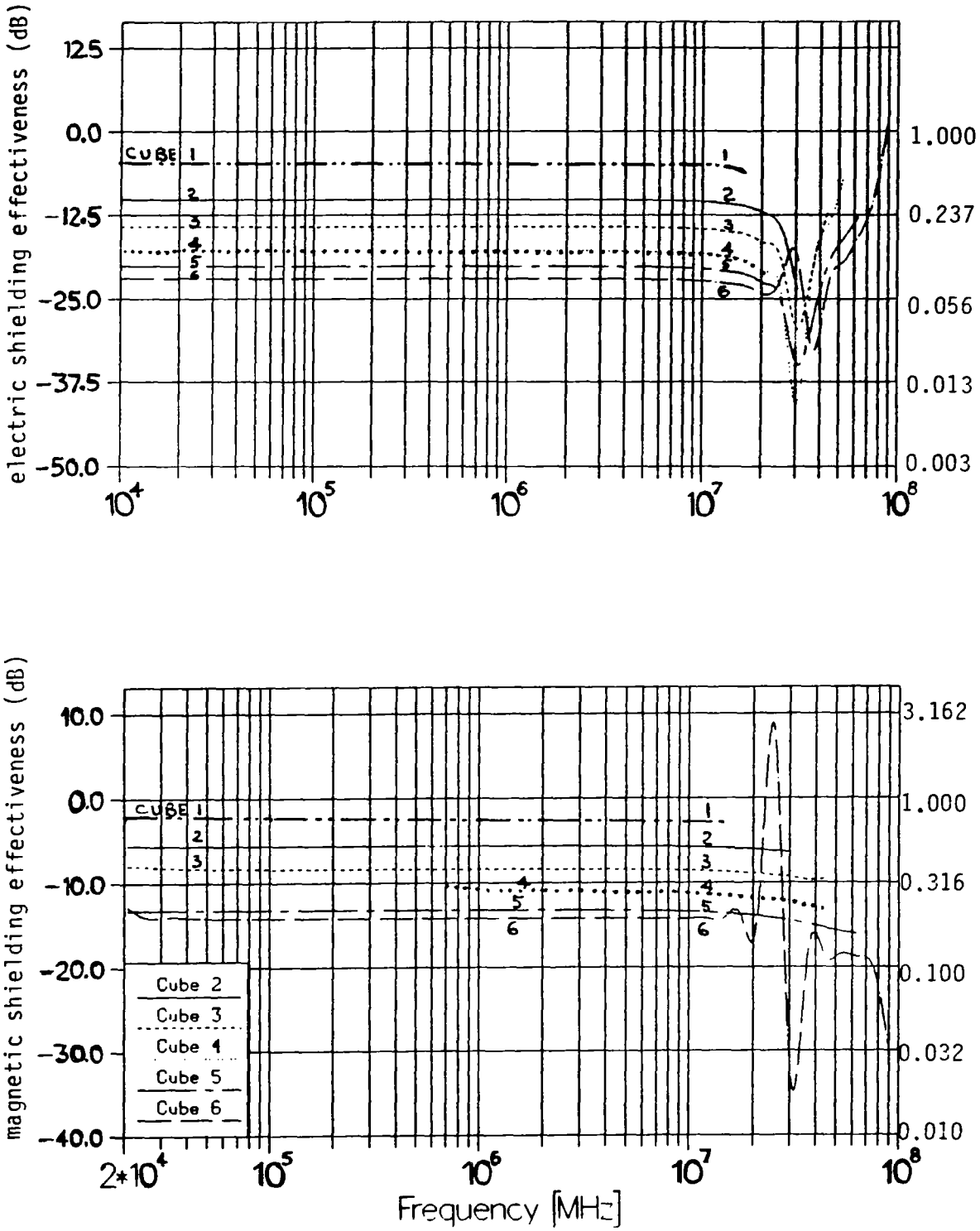

Figure 11. Electric and magnetic shielding effectivenesses computed as a function of frequency at the center of CUBE - N.
(2m cube with N segments per edge; see figure 3a for incidence angle and polarization)

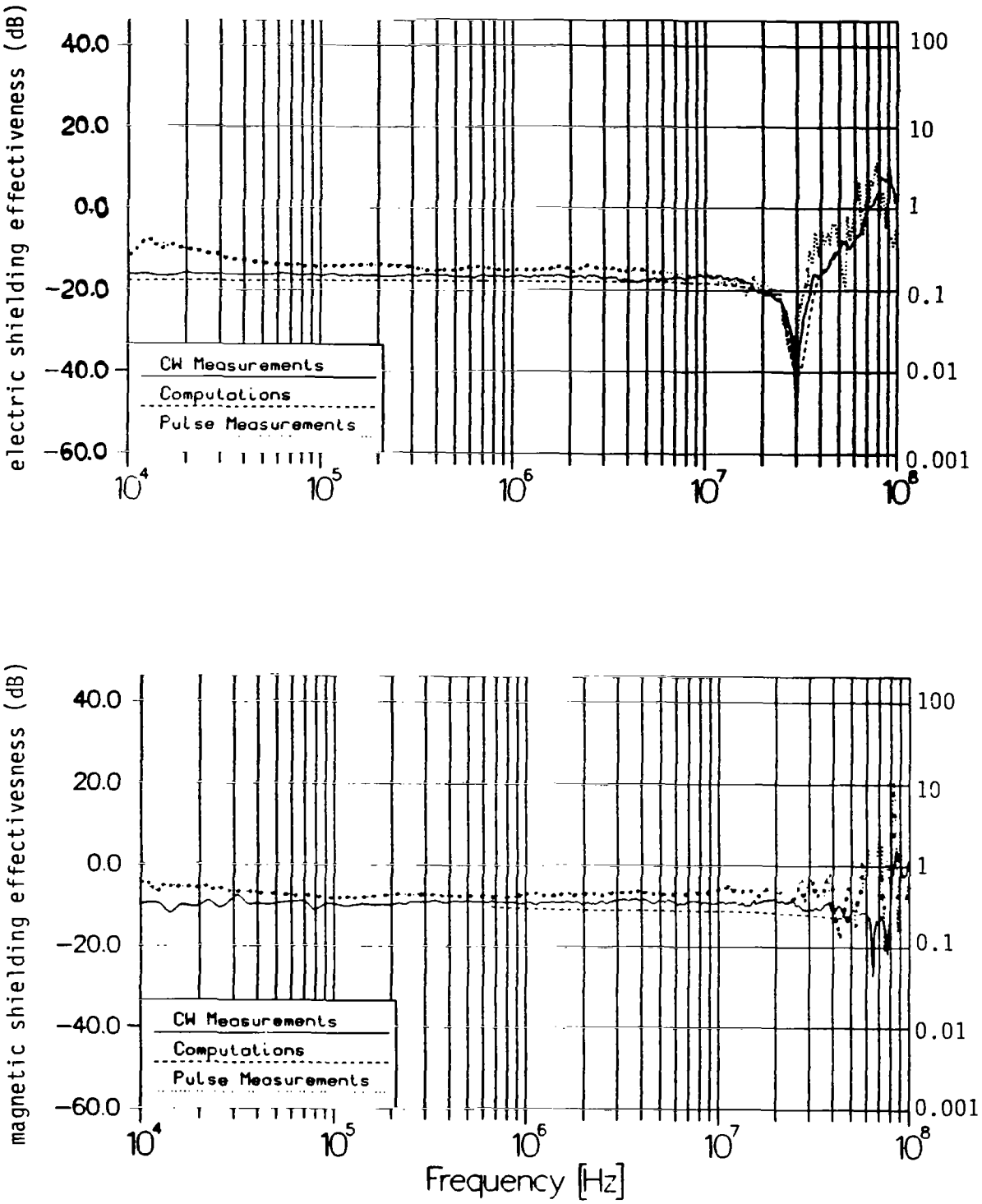

Figure 12. Electric and magnetic shielding effectivenesses computed and measured (CW & pulse) for CUBE-4
(2m cube with 0.5m segmentation, 192 segments)
(see figure 3a for incidence angle and polarization)

Figure 13 and 14 respectively deal with the 2 m long cylinder (2 m diameter; 0.4m segment for a total of 272 segments) for the two polarizations of the incident electric and magnetic fields being parallel to the cylinder axis. Once again, the electric shielding effectivenesses are superior to the magnetic quantities, in general. The notch in the frequency domain for the electric shielding effectiveness is seen to be at about 25 MHz, corresponding to a wavelength of 12 m.

Figures 15 and 16 resspectively deal with the 4m long cylinder (2m diameter; 0.4m segments for a total of 432 segments) for the two polarizations, as in the case of 2 m cyl inder above. The notch in the electric shielding effectiveness at the center of the cylinder is now seen to be at about half this frequency, observed for the 2m cylinder.

7. Summary

The problem of electromagnetic field interaction with wire cage structures has been addressed in this note. Canonical shapes e.g., cubes and cylinders that are formed by wire segments are considered in this study. The electric and magnetic shielding effectivenesses are both computed and measured . The computations are performed using Numerical Electromagnetic Code(NEC-2) which solves the electric field integral equation (EFIE), under a thin wire approximation for the current distributions on all wire segments. The current is assumed to be a sum of three terms consisting of a constant, sine and cosine terms. Junction conditions and the method of moments equations are then used in solving for the currents from which the near electric and magnetic fields are estimated. It is then a simple matter to evaluate the total fields as a vector sum of scattered and incident fields, and finally the shielding effectivenesses as a function of frequency. All of the restrictions on segment lengths are strictly adhered to. The shielding effectivenesses are also experimentally measured in a hybrid type of EMP simulator, the Swiss MEMPS, when it is energized by both a broadband or swept CW source and a transient pulse generator. Incident and total fields are measured in both cases and shielding effectivenesses estimated. In the case of pulse measurements, the fields are Fourier transformed before estimating the shielding effectivenesses. Certain errors get introduced at low frequemcies in the Fourier transformation, due to the lack of late - time data. In the frequency range of 100 kHz to 50 MHz , the agreement between calculations and experiments is seen to be good.

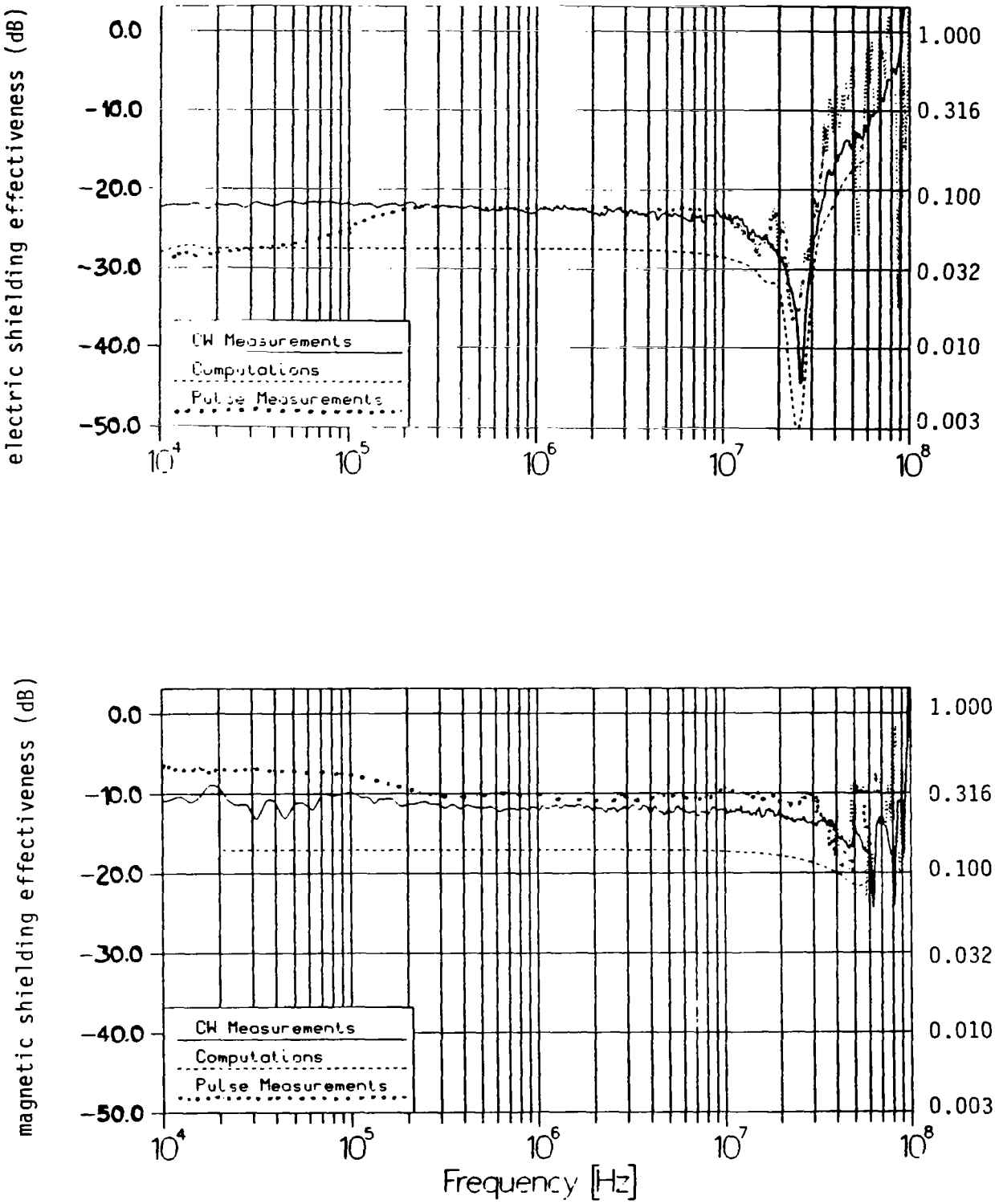

Figure 13. Electric and magnetic shielding effectivenesses computed and measured (CW & pulse) at the center of a 2m long , 2m diameter cylinder (incident electric field parallel to the axis)

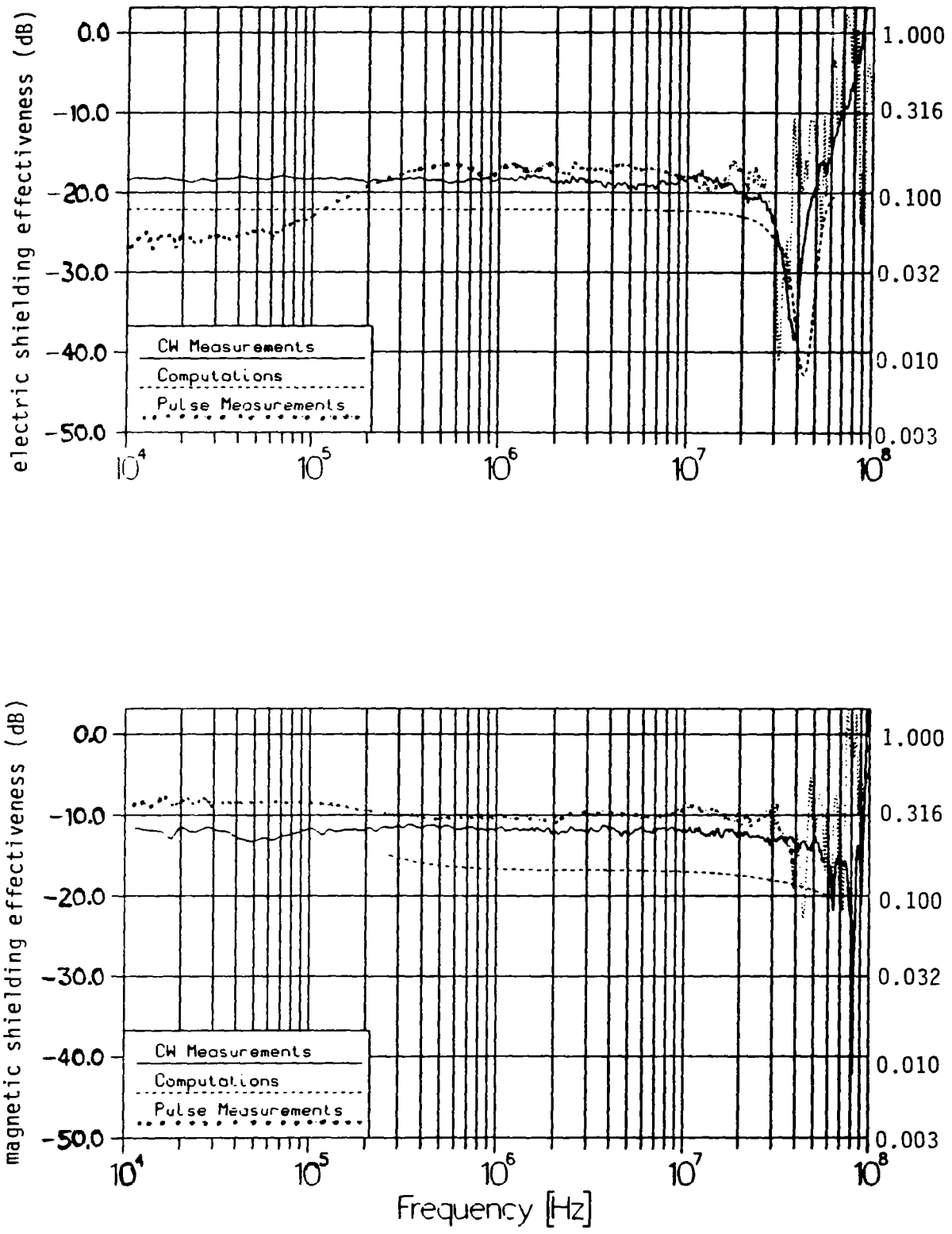

Figure 14. Electric and magnetic shielding effectivenesses computed and measured (CW & pulse) at the center of a 2m long and 2m diameter segmented cylinder (incident magnetic field parallel to the cylinder axis)

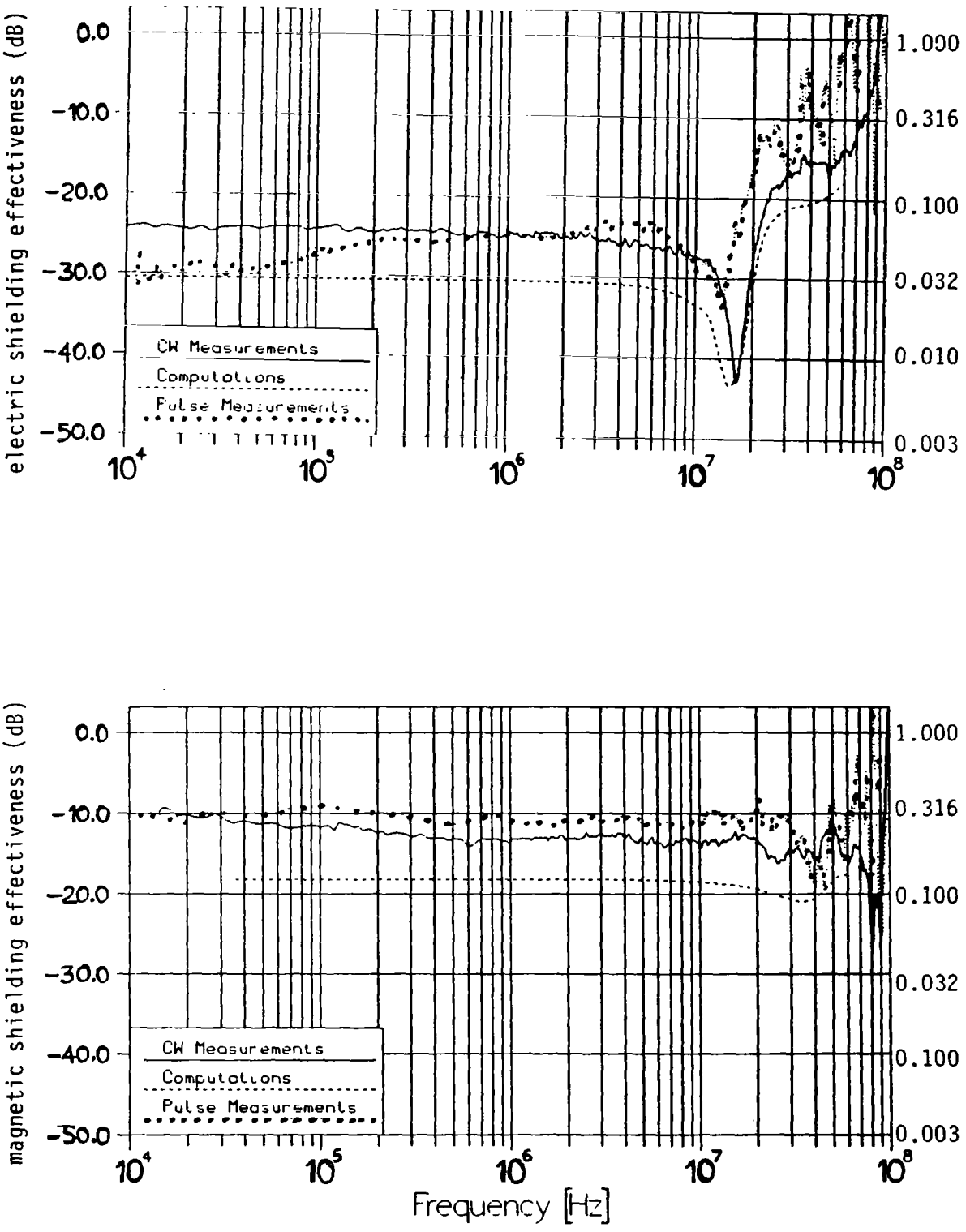

Figure 15. Electric and magnetic shielding effectinesses computed and measurde (CW & pulse) at the center of a 4m long, 2m diameter segmented cylinder (incident electric field parallel to the cylinder axis)

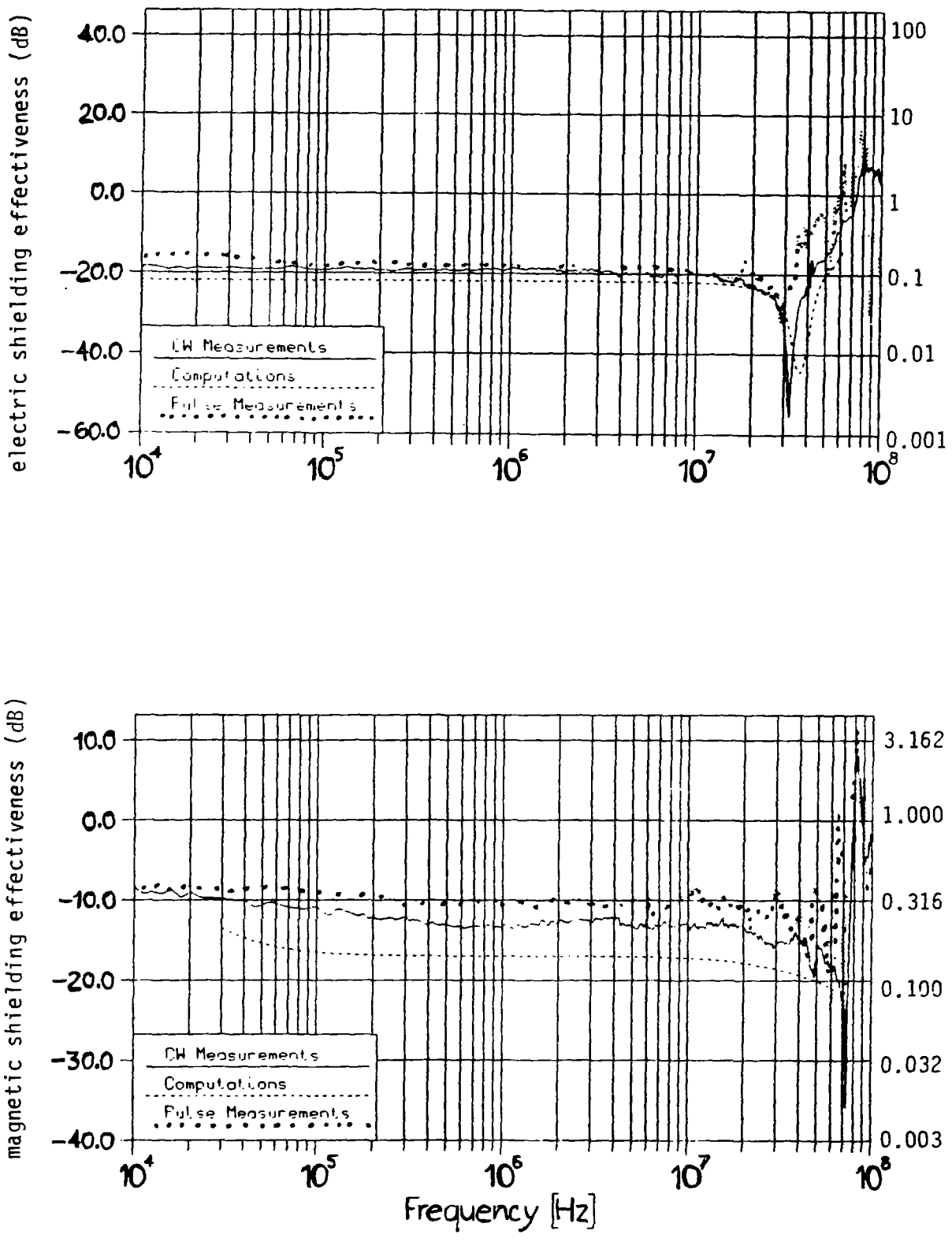

Figure 16. Electric and magnetic shielding effectivenesses computed and measured (CW & pulse) at the center of a 4m long, 2m diameter segmented cylinder (incident magnetic field parallel to the cylinder axis)

References

[1] C.E.Baum, "EMP Simulators for Various Types of Nuclear EMP Environments: An Interim Categorization", Sensor and Simulation Note 240, January 1978; also as special issues on Nuclear Electromagnetic Pulse in IEEE Transactions on Antennas and Propagation, January 1978, pp. 35-53, and IEEE Transactions on Electromagnetic Compatibility, February 1978, pp. 35-53.

[2] K.S.H.Lee (editor), "EMP Interaction: Principles, Techniques and Reference Data," Hemisphere Publishing Corporation, New York, 1986.

[3] M.I.Kontorovich, V.Yu. Petrun'kin, N.A. Yesepkina, and M.I. Astrakhan, "The Coefficient of Reflection of a Plane Electromagnetic Wave from a Plane Wire Mesh," Radio Engineering and Electronic Physics, volume 7, number 2, 1962, pp. 222-231.

[4] D.A.Hill and J.R.Wait, " Electromagnetic Scattering of an Arbitrary Plane Wave by a Wire Mesh with Bonded Junctions," Canadian Journal of Physics, Volume 54, 1976, pp. 353-361.

[5] D.A.Hill and J.R.Wait, " Theoretical and Numerical Studies of Wire Mesh Structures," Sensor and Simulation Note 231, 10 June 1977.

[6] J.R.Wait and D.A.Hill, " Electromagnetic Scattering by Two Perpendicular Wire Grids Over a Conducting Half Space," Radio Science, Volume 11, Number 8,9, August -September 1976 pp. 725-730.

[7] A.A.Smith,Jr., " Attenuation of Electric and Magnetic Fields by Buildings, " IEEE Trans. on Electromagnetic Compatibility, Volume EMC-20, Number 3, August 1978, pp. 411-418.

[8] A.Reineix, A.Boijaud and B.Jecko, " Electromagnetic Pulse Penetration Into Reinforced-Concrete Buildings, IEEE Transactions on Electromagnetic Compatibility, Volune EMC-29, Number 1, February 1987, pp. 72- 78.

[9] M. Z. Netzer, " Architectural Shielding: Upgrading the Natural Shielding Effectiveness of Reinforced Buildings, " ITEM update 1988, starting on page 14.

[10] G.J.Burke and A.J.Poggio, " Numerical Electromagnetic Code User's Guide", NOSC Tech. Document 116, Volume 2, Part III, also Lawrence Livermore Laboratory Report, UCID - 18834, 1981.

[11] G.J.Burke, " The Numerical Electromagnetic Code (NEC)", in Applications of Method of Momemts to Electromagnetic Fields , edited by B.J.Strait, Pergamon Press, 1973.

[12] A.G.Poggio and E.K.Miller, " Integral Equation Solutions of Three- dimensional Scattering Problems", in Computer Techniques for Electromagnetics, edited by R.Mitra, Pergamon Press, 1973, pp. 159-264.

[13] J.H.Wang, " Generalized Moment Methods in Electromagnetics," John Wiley and Sons,1991

[14] Y.S.Yeh and K.K..Mei., " Theory of Conical Equiangular Spiral Antennas, " Part I-Numerical Techniques," IEEE Transactions on Antennas and Propagation., volume AP-15, 1967, p. 634

[15] D.V.Giri, J.Fang, P.Mani and M.Nyffeler, " Near Fields of an Impedance-Loaded Elliptical Antenna," Proceedings of the 9th International Zurich Symposium and Technical Exhibition on Electromagnetic Compatibility, 12-14 March 1991, pp. 363-366.

[16] D.Hansen , H.Schaer, D.Koeningstein, H.Hoitink and D.V.Giri, " Response of an Overhead Wire near an NEMP Simulator, " IEEE Transactions on Electromagnetic Compatibility, vol. EMC-32, Number 1, February 1990.

[17] K.F.Casey and E.F.Vance, " EMP Coupling Through Cable Shields", Joint Special Issue on the Nuclear Electromagnetic Pulse, IEEE Transactions on Antennas and Propagation, January 1978, pp. 100-106, and in IEEE Transactions on Electromagnetic Compatibility, February, 1978, pp. 100-106.